The role of salinity in the decadal variability of the North Atlantic meridional overturning circulation

Claude Frankignoul
LOCEAN / IPSL, Université Pierre et Marie Curie - Paris 6, case 100, 4 place Jussieu, 75252 Paris Cedex 05, France

Julie Deshayes, and Ruth Curry
Woods Hole Oceanographic Institution Woods Hole, Mass O2543, USA

To appear in Climate Dynamics

Abstract

An OGCM hindcast is used to investigate the linkages between North Atlantic Ocean salinity and circulation changes during 1963–2003. The focus is on the eastern subpolar region consisting of the Irminger Sea and the eastern North Atlantic where a careful assessment shows that the simulated interannual to decadal salinity changes in the upper 1500 m reproduce well those derived from the available record of hydrographic measurements. In the model, the variability of the Atlantic meridional overturning circulation (MOC) is primarily driven by changes in deep water formation taking place in the Irminger Sea and, to a lesser extent, the Labrador Sea. Both are strongly influenced by the North Atlantic Oscillation (NAO). The modeled interannual to decadal salinity changes in the subpolar basins are mostly controlled by circulation-driven anomalies of freshwater flux convergence, although surface salinity restoring to climatology and other boundary fluxes each account for approximately 25% of the variance. The NAO plays an important role: a positive NAO phase is associated with increased precipitation, reduced northward salt transport by the wind-driven intergyre gyre, and increased southward flows of freshwater across the Greenland-Scotland ridge. Since the NAO largely controlled deep convection in the subpolar gyre, fresher waters are found near the sinking region during convective events. This markedly differs from the active influence on the MOC that salinity exerts at decadal and longer timescales in most coupled models. The intensification of the MOC that follows a positive NAO phase by about 2 years does not lead to an increase in the northward salt transport into the subpolar domain at low frequencies because it is cancelled by the concomitant intensification of the subpolar gyre which shifts the subpolar front eastward and reduces the northward salt transport by the North Atlantic Current waters. This differs again from most coupled models, where the gyre intensification precedes that of the MOC by several years.

1 Introduction

Ocean salinity distributions have exhibited extensive changes on decadal and longer time scales. During the last four decades, upper ocean salinities increased substantially in the tropical and subtropical Atlantic. Over this same period, the water column in the high latitude North Atlantic exhibited 30-years of steady freshening, which then reversed in the last half of the 1990s (e.g., Curry et al. 2003; Curry and Mauritzen 2005; Peterson et al. 2006; Boyer et al. 2007). The freshening of the Nordic Seas and subpolar basins, where a substantial part of the dense, deep waters of the world ocean are formed, was associated with an amplification of the NAO from its low phase in the 1960s to its opposite extreme in the early 1990s. This was punctuated by events such as the "Great Salinity Anomaly" (GSA, Dickson et al 1988) of the early 1970s, but more generally involved enhanced net precipitation, river discharge, melting ice stocks, and exchanges with the Arctic (Peterson et al. 2006).

Since a decrease in the surface salinity (hereafter SSS) decreases the density and hinders deep convection, simple reasoning suggests that, in the absence of other effects, it should weaken the Atlantic meridional overturning circulation (MOC). This holds in global climate models under strong external forcing, as shown by the weakening of the MOC in response to a large freshwater input at high latitude (e.g., Vellinga and Wood 2002) or to increased high latitude precipitation and temperature in global warming conditions (e.g., Bryan et al. 2006). Whether the smaller salinity changes that occur in the absence of strong external forcing significantly impact the MOC is more difficult to establish. The observational record is too sparse to estimate low-frequency changes in the MOC, while simulations of the 20th century variations indicate that the recent high latitude freshening, was accompanied by a slow MOC increase (Wu et al. 2004), possibly reflecting the large natural variability of the MOC.

Under control conditions, climate models also exhibit substantial MOC fluctuations that critically involve salinity changes. In the Geophysical Fluid Dynamics Laboratory (GFDL) R-15 model, the Atlantic MOC varied substantially at 40 – 60 yr period (Delworth et al. 1993). During a phase of weak MOC, reduced northward heat transport built a pool of cold, dense upper waters in the middle North Atlantic. This progressively increased the cyclonic subpolar gyre circulation and salt transport into the convection region, which after a few years strengthened the MOC and its northward heat transport, leading to a phase reversal of the oscillation. Reduced freshwater transport from the Arctic also contributed to

the salinity increase in the convective region (Delworth et al. 1997). Sensitivity studies by Delworth and Greatbach (2000) showed that these multidecadal MOC fluctuations largely reflected the passive response of the ocean to the "natural" variability of the surface heat fluxes, in particular those associated with the North Atlantic Oscillation (NAO).

Broadly similar mechanisms are at play in control simulations of several more recent, higher resolution climate models, although with different dominant periods. In HadCM3, a dominant period is shorter (25 yr), but the sequence of events similar, with the ocean setting the time scale and salinity playing an active role (Dong and Sutton 2005). Salinity is the main driver of the Atlantic MOC in IPSL-CM4, where the dominant period is 15-20 yr (Msadek and Frankignoul 2008). Salinity also plays a key role at centennial periods in HadCM3 (Velinga and Wu 2004, Hawkins and Sutton 2007), but with a larger influence of convection in the Nordic Seas and freshwater exchanges with the Arctic, similar to the 70-80 yr fluctuations in ECHAM5/MPIOM (Jungclaus et al. 2005). Key to the MOC variability in these coupled models is the horizontal transport of salt into the convective regions and its strong influence on deep convection, a substantial phase lag between gyre and MOC changes, and, when there is a spectral peak, the role of the MOC-induced meridional heat transport to reverse the phase of the oscillations. In a few cases, however, temperature dominates the subpolar density fluctuations, as in the 30-yr variability of a lower resolution version of ECHAM5/MPIOM, which seems to be an ocean internal mode (Zhu and Jungclaus 2008)

While the observational record is insufficient to document MOC changes, the role of salinity and the link between MOC and gyre changes can be tested with ocean general circulation model (OGCM) hindcasts. The OGCMs generally are of higher resolution and are forced by more realistic atmospheric fields. Compared to coupled models, they typically provide a better representation of observed watermasses and circulation, particularly in regions of deep convection. However, the hindcasts are limited to approximately the last 50 years and thus do not resolve multidecadal variations, and they often require a restoring toward an observed SSS climatology to reduce model drifts in salinity.

Most OGCM hindcasts show some skill at reproducing observed oceanic changes at high latitude, and have consequently been used to investigate links between salinity and MOC changes. Simulations of large events such as the GSA of the early 1970's show contrasting results. Häkkinen (1999) found in a regional model with no surface salinity restoring that GSAs strongly reduced the deep convection in the Labrador Sea and weakened the Atlantic MOC by up to 20%. Haak et al. (2003) found in a higher resolution

model with weak salinity restoring that convection in the Labrador Sea was only reduced for a few years and the Atlantic MOC was barely affected. There is thus a need to further investigate the influence of salinity changes on the MOC in OGCM hindcasts and to determine whether those salinity variations play an active role at the decadal scale, as suggested by coupled models, or behave primarily as a passive tracer. Before asserting parallels between the dominant mechanisms at play in these hindcast models and the real climate system, thorough assessments must be undertaken of a model's strengths and weaknesses in reproducing the observed circulation and salinity features.

In this paper, we investigate the role of salinity in Atlantic MOC variability on interannual to decadal timescales using a hindcast with a nested regional ocean-ice model. The simulation has been used in a number of studies which noted favorable comparisons with hydrographic observations, in spite of diminished exchanges of dense waters between the Nordic Seas and the subpolar domain (e.g., Hátún et al. 2005; Mauritzen et al. 2006). In the model, the MOC is primarily driven by deep convection in the subpolar gyre (Deshayes and Frankignoul 2008, hereafter DF08). We thus focus on the relation between the salinity changes in the subpolar gyre, deep convection, and the North Atlantic circulation. An independent study by Mauritzen et al. (2006, hereafter MHS), based on the same model output, was published during the course of this study, and there is some unavoidable overlap with their analysis. However, we focus here on complementary aspects, carefully assessing how the model reproduces the observed salinity changes and discussing the influence of the surface salinity restoring. We find relationships among upper ocean salinity, the subpolar gyre circulation, and the MOC which differ distinctly from those diagnosed in most coupled climate model simulations.

2. The simulation

We consider a hindcast simulation of the North Atlantic Ocean using a regional version of the Nansen Center version (Bentsen et al. 2004) of the Miami Isopycnic Coordinate Ocean Model (MICOM, Bleck et al. 1992. Detailed descriptions of the model, its circulation and water property characteristics have been previously published (e.g., Drange et al., 2005; Hatun et al. 2005a and b; Mauritzen et al. 2006; Deshayes et al. 2007; DF08). We refer the interested reader to these sources, and provide a more brief description here.

A regional model spanning about 30°N to 78°N with resolution of 20 km is relaxed at the (approximately) meridional boundaries to a global simulation using the same model, but

at half the resolution (40 km). The Strait of Gibraltar is closed. The model has 26 density layers in the vertical and includes sea ice dynamics. The 40 km global simulation was forced for the 1948-2003 period by freshwater, heat and momentum fluxes derived from the NCEP reanalysis (Kalnay et al. 1996) employing the scheme of Bentsen and Drange (2000) which includes realistic run-off and a freshwater correction flux, after a 85-year spin-up phase (30 years with monthly mean atmospheric forcing followed by one full cycle with NCEP daily forcing). The finer resolution regional model was similarly forced by NCEP-derived fluxes, but mixed layer temperature and salinity were additionally relaxed (in ice-free regions) onto the sea surface temperature (SST) and the SSS climatologies of Levitus et al. (1994) and Levitus and Boyer (1994), respectively. An e-folding relaxation time was set to 30 days for a 50 m thick mixed layer, and reduced linearly where it exceeded 50 m. Relaxation was limited to a maximum SST and SSS difference of 1.5°C and 0.5 psu, respectively, to avoid obliterating water properties in regions with large model circulation biases (such as the position of the North Atlantic Current). Air-sea fluxes were (unfortunately) not saved during the simulation. We focus on 1963-2003, the time period for which the simulation appears to have adjusted to the time-varying atmospheric forcing and come into alignment with the observational record.

2.1 Mean Circulation

The bathymetry of the study region is shown in Fig.1. The mean circulation of the regional model closely parallels observations in the Labrador and Irminger Seas (Lavender et al. 2000, Reverdin et al 2003), exhibiting maximum intensities in the boundary currents that follow topography (i.e. the East Greenland, West Greenland, and Labrador Currents). Since these boundary currents feature decreasing amplitude with depth and virtually no change in direction, the mean barotropic streamfunction (hereafter BTSF) provides a practical proxy for the total mean circulation (Fig. 2). The amplitude and geography of the simulated gyre circulation are quite realistic, e.g. ~40 Sv South of Cape Farewell, Greenland, while well-documented recirculation cells are also reproduced, e.g. between the Labrador Sea and Irminger Seas.

The model's convection characteristics have been described by Deshayes et al. (2007, hereafter DFD) and are briefly summarized here. The timing and magnitude of dense water production strongly resemble what has been observed, however the details of location and convection depth differ to some degree. In the hindcast, classic Labrador Sea Water (cLSW) was formed by deep convection in the Labrador Sea near 58°N, 55°W, close to the

observed one, and in the Irminger Sea near 64°N, 31°W, (Fig. 1). The latter is northeast of the location suggested by observations and closer to the boundary current (e.g., Pickart et al. 2003, Falina et al. 2007). Similar to the observational record, simulated deep convective events occurred in the Labrador Sea during the years 1972, 1983, 1984, 1989-1991 and 1993, in conjunction with anomalous heat fluxes and positive phases of the NAO (Fig. 3). NAO heat fluxes also affected overturning in the Irminger Sea about 1 year later, but there, preconditioning associated with intensification of the cyclonic boundary current played a dominant role. Approximately 4 Sv of cLSW was formed every year in the Irminger Sea, which seems overly large although no estimate has been derived from observations. Newly formed deep waters rapidly exited the Irminger Sea where the convection occurred near the boundary currents. The rate of formation of cLSW in the Labrador Sea during deep convection events averaged to 8 Sv, which corresponds well to observations (e.g. Rhein et al. 2002).

The simulated circulation also reveals certain deficiencies and biases. The subtropical gyre is too weak (owing to coarser resolution near the southern boundary of the regional model), the North Atlantic Current (NAC) is located too far south, and eddy activity is strongly damped. The southward transport of dense overflow waters exiting the Nordic Seas for $\sigma_\theta \geq 27.8$ is only ~2.3 Sv -- less than half of the ~6 Sv that has been observed (e.g., Dickson and Brown 1994). This results in a weakened mean North Atlantic MOC (~11 Sv at 44°N[1], Fig. 4) compared to more generally accepted values (15 and 14 Sv at 47°N in Ganachaud and Wunsch 2000 and Lumkin and Speer 2003, respectively). MHS, however, noted that the observed inflow of about 8 Sv of warm Atlantic waters to the Nordic Seas is very well represented. Finally, the Antarctic Bottom Water (AABW) cell is not reproduced, a common defect of isopycnal coordinate models (Willebrand et al. 2001).

2.2 Circulation Variability

The first empirical orthogonal function[2] (EOF) of the MOC indicates that its variability is strongly dominated by modulation of its strength (typically 2 Sv). The (normalized) principal component of this mode provides an MOC index (MOC PC1). This describes a generally weak MOC prior to 1970, followed by intensification to peak values in the early 1990s, and diminishing thereafter (Fig. 4, lower panels). This is similar to the behavior of

[1] In the global model, the Atlantic MOC is stronger, reaching 16 Sv at 44°N.
[2] We use rotated EOFs. Rotation has no perceptible effect on MOC or BTSF EOF1, but slightly improves the representation of the NAO-driven intergyre circulation by EOF2.

other OGCM hindcasts (e.g., Eden and Willebrand 2001; Bentsen et al. 2004; Böning et al. 2006). MOC PC1 is well correlated (r= 0.73 for the period 1953-2003, after linear detrending) with the dense fraction of the DWBC in the Labrador Sea (DF08). It is primarily affected by deep water production in the Irminger Sea and is well correlated (r = 0.5) with the Irminger convection index from Fig. 3 -- both in phase and, to a lesser extent, lagging it by 1 year (DF08). The correlation with convection in the Labrador Sea is smaller and the time lag larger. Hence, the simulated MOC reaches a maximum intensification about 2 years after a positive NAO phase.

The main mode of variability in the horizontal circulation implies a strengthening (in this polarity) of both the subpolar and subtropical gyres (Fig. 2). Its time evolution (BTSF PC1) is discussed in Hátún et al. (2005a), MHS, and DF08. It tends to lag the NAO by 2 years, and is broadly consistent with the transport indices of Curry and McCartney (2001) and the altimetry data of Häkkinen and Rhines (2004). BTSF PC1 is well correlated with MOC PC1 (all correlations are given for linearly detrended data, even though the trend is not removed when displaying the time series), such that the strengthening of the Atlantic MOC after a positive NAO phase is accompanied by an intensification of the subpolar and subtropical gyres (Fig. 5). However, the gyres seem to stabilize by the end of the 90s while the MOC keeps weakening. The second mode of BTSF variability is an intergyre circulation (Fig. 2). This primarily reflects the barotropic response of the North Atlantic to the NAO wind stress curl and is thus well correlated (r = 0.6) with the NAO index -- even on the monthly time scale.

A key feature of this hindcast, discussed in more detail in DF08, is that the dominant changes in the Atlantic MOC, namely its intensification or weakening, occur broadly in phase with the intensification or weakening of the subpolar gyre, a strengthening of the two circulations occurring about 2 years after a positive NAO phase. Most OGCM hindcasts exhibit a similar phase relation (e.g., Eden and Willebrand 2001; de Cöetlogon et al. 2006; Böning et al. 2006). Eden and Young (2001) found that the lag with the NAO increased on interdecadal timescales, but that the MOC and gyre circulation remained approximately in phase. Hence, OGCM hindcasts differ fundamentally from the coupled models discussed in Section 1, where the intensification of the subpolar gyre precedes that of the MOC by several years.

3. Salinity changes in the subpolar gyre

Before addressing the role of salinity in MOC changes, we candidly assess how well the model represents the mean salinity distribution and its temporal variability. Previous studies (Hátún et al. 2005a and b) demonstrated that this model capably reproduced variations in near-surface temperature and salinity on seasonal, interannual and decadal timescales – at least in the vicinity of the Iceland-Scotland Ridge since 1994 and along the Rockall Trough after 1975. MHS noted strong similarities between observed and simulated trends and interannual changes in full-depth freshwater storage anomalies in the subpolar basins. Here we further evaluate the time evolution of observed and simulated salinity fields for three broad regions of the subpolar domain through direct comparisons with the available record of hydrographic measurements using Hydrobase (Curry 2002). As documented next, we find that despite systematic fresh biases throughout the water column, the amplitude changes of simulated salinity distributions are consonant with the observed changes from the mid-1960s onward (prior to 1963, there is little correspondence between the observed and simulated records, presumably because of insufficient time for water mass adjustment). We conclude that the observed variability in both salinity and circulation is reproduced well enough to justify using the model to investigate linkages between them on interannual to decadal timescales.

3.1 Mean fields

The model's mean upper ocean salinity distributions are quite realistic, beyond certain circulation biases noted in Section 2. For example, the Gulf Stream is too close to the coast, the NAC is too far south, and the ultra-fresh waters of the Labrador Current extend too far eastward into the interior (see Fig. 8 below). To some extent, such accuracy is expected from relaxing the model to climatological surface values.

Beneath the sea surface, the main observed watermass and circulation features are also reproduced by the simulation. This is illustrated along a section running west to east across the subpolar basins near 55°N (location in red, Fig. 1) sliced similarly (but not exactly) through the simulated and observed density and salinity fields averaged for the period 1963–2002 (Fig. 6). Saline subtropical inflows in the eastern basins contrast with very fresh surface waters of Arctic origin in the west, a salinity minimum corresponding to LSW occupies the mid-depths and overlies a slighty more saline watermass reflecting the Nordic Seas overflows.

Some departures from reality are also evident in these sections: salinities are significantly lower in the simulation and the structure of the deep overflow layers differs from what is observed. The interior subpolar watermasses are about 0.25 psu too fresh (compensated by the water being 2 to 3°C too cold, see DFD). This implies an overall deficiency in the sources of warm, saline waters to these basins, and must certainly reflect the closure of the Mediterranean and omission of its warm, saline outflows at mid-depths (> 800 m) in the nested simulation. Inherent to isopycnal models are characteristics that dampen eddy fluxes from the boundary and inhibit restratification (Eldevik 2002; Rousset et al. 2007), which may also contribute to fresher, colder basin interiors.

In the deep layers, the simulated density and salinity structure reflect the difficulties of isopycnal coordinate models in reproducing the processes of overflow and entrainment that ventilate these deep basins (e.g., Willebrand et al. 2001). The volume of dense waters (σ_θ> 27.80 kgm^{-3}) corresponding to the overflows is significantly reduced and the salinity maximum observed below 2 km is replaced by a small salinity increase down to the bottom. As a consequence, the overlying watermasses produced by deep convection (for example cLSW, σ_θ=27.74–27.78 kgm^{-3}) reach deeper in the water column than what is observed. Furthermore, most of the Iceland-Scotland Overflow Water (ISOW) exiting the Nordic Seas continues southward into Rockall Trough and the deep eastern North Atlantic basins, rather than flowing west through the Faeroe Bank Channel into the Iceland Sea and western subpolar basins. In the 55°N sections, a patch of dense, saline waters beneath 2300 m in the easternmost basin reflects this situation. We speculate that the reduced westward flow of ISOW prevents development of a salinity maximum in the overflow layers of the western basins.

3.2 Variability of salinity

Comparing the timelines of observed and simulated salinity changes in three broad regions of the subpolar domain (locations denoted in Fig 1), provided essential confidence that this hindcast reproduced similar amplitudes of variability. To compare the simulations and observations in each region, timeseries of volume-weighted average salinity, binned in 5-year time periods, were estimated for each of four vertical layers (Fig. 7). Prior to 1965, the simulated salinities bear little resemblance to the observations, but the spin-up was too short for watermass adjustment, and the 1953-1962 period was therefore excluded from further study (and from further discussion here). From 1965, the upper three layers (spanning 0–1500 m) of the observational record exhibited high salinities in the late 1960s,

a sudden decline in the early 1970s to a protracted phase of relatively fresh conditions, and a recovery to high salinities in the mid 1990s. For the deepest layer (> 1500 m), the observed decline and rise was more muted, but still evident.

The simulated and observed variability compare most favorably in the Irminger (IRM) region, although the freshwater influx in the early 70s is slightly underestimated (Fig. 7). This event, labeled the GSA, has been attributed to enhanced Arctic exports of sea ice and freshwater plus strong local precipitation anomalies (Dickson et al. 1988; Peterson et al. 2006). The interior Labrador basin (LAB) does not reproduce the freshwater decline observed in the upper ocean from 1965 to 1975 (nor the post-1995 increase), but does echo the slow accumulation of freshwater observed at depths > 1500 m. The weakness of the freshening from 1965 to 1975 is largely due to the strong underestimation in the model of the Arctic exports of sea ice and freshwater in the late 60s, which lead to the appearance of the GSA in the Labrador Sea (Dickson et al. 1988, Belkin et al. 1998). The lack of freshwater pulse from the Arctic could also explain the slight underestimation of the freshening in IRM and ENA, even though the precipitation increase in the mid-70s seems well represented in the NCEP reanalysis (Josey and Marsh 2005, Peterson et al. 2006). In the eastern basins (ENA), the simulation does not quite capture the same amplitude of high salinities that were observed from 1963 to 1973, in particular between 500 and 1000m, but does reproduce well the salinity increase of the 1990s. About 40% of the observed freshwater flux anomaly increase in the eastern subpolar domain (IRM + ENA) between the 5-yr periods centered around 1970 and 1975 is missing (260 mSv versus 453 mSv), mostly in the ENA region. It could be due to a combination of factors: inaccurate air-sea fluxes, inadequate representation of the freshwater and sea-ice transport across the domain boundaries, lateral mixing, and observational uncertainties. In the deepest layer of all three regions, the simulation exhibits a salinity decline through time, which was observed in IRM and LAB regions, but not in ENA. The salinity decrease in IRM and LAB is consistent with the observed one below 1500 m, suggesting that it is not due to model drift, although it cannot be excluded that the latter also contributed. The simulated freshening in ENA's deep layer reflects a stronger influence of ISOW in the model's eastern basins (ISOW flows southward through Rockall Trough instead of westward into the Irminger and Labrador basins) – and the 30-year freshening of these overflows that was observed since the 1960s (e.g. Dickson et al. 2002). This discrepancy of deep watermass distribution in the deep eastern basins, however, does not adversely influence this investigation that concerns mainly the upper ocean and overturning circulations.

From these comparisons we conclude that the simulated variability of salinity distributions in the subpolar regions spanned by IRM and ENA is adequate for investigating dynamical interactions between salinity, the gyre circulation and MOC in the model after 1963. The observed low frequency salinity fluctuations are broadly reproduced in the upper layers (0-1500 m) of these regions. The hindcast also faithfully reproduced the freshening of the overflows and the subpolar watermasses produced by deep convection which has been observed for the years 1970-2000.

An additional view of the simulated salinity changes supports our conclusion. The upper ocean salinity distributions and anomaly fields from the simulation and observational record are compared for the extremes of the salinity fluctuation – the time periods 1973-77 and 1998-02 (Fig. 8 and 9). In the earlier time period, the NAO was predominantly positive and the subpolar front was in an eastward position: the high salinity signature of subtropical inflows was restricted to the region east of 20°W in the eastern subpolar domain (Fig. 8, left panels). By contrast, in 1998-02 when the NAO had retreated to a negative or neutral phase, the subpolar front was retracted westward, and saline inflows extended further into the subpolar basins (see also Bersch 2002; Flatau et al. 2003). These images confirm that, in the subpolar domain, circulation and salinity distributions are closely related. Moreover, the close correspondence between the simulated and observed fields affirms that this GCM is an appropriate tool for investigating the underpinnings of that linkage.

4. The freshwater budget of the eastern subpolar gyre

To investigate the causes of the salinity changes, we consider the freshwater budget of the eastern subpolar region from 1963 to 2003 in the hindcast, when the simulated salinity anomalies resembled observations (Fig. 6). The domain, limited to the south by section A25 and to the north by the Greenland-Scotland ridge (section OFLW), plus the Channel section (Fig. 1), does not include the Labrador Sea, which is briefly discussed in section 5, but combines the Irminger Sea (IRM), which is key to the simulated MOC variations, and the eastern North Atlantic (ENA). The freshwater content is determined by a balance between the freshwater exchanges at the air-sea interface, run-off, ice melting, horizontal mixing, and freshwater transport across the lateral boundaries. The freshwater transport convergence was calculated from the model output, but the other fluxes could not be calculated from the data that were saved during the simulation. Hence, we estimated them by a residual calculation and, for the salinity restoring, by an approximate calculation based

on monthly SSS and mixed-layer depth data. An accurate calculation would require daily data, but the monthly ones should provide acceptable estimates.

The freshwater transport across a section is given at time t by

$$\int \int F(x,z,t)\, v(x,z,t)\, dx\, dz \qquad (1)$$

where F is the freshwater $(S_0\text{-}S)/S_0$, with S_0 = 34.8 (the reference salinity for the Arctic used by Cuny et al. 2005), v is the velocity normal to the section, x is the location along the section and z the depth. Time series of the yearly northward freshwater transport across section A25 and the southward one across section OFLW were calculated using monthly data. The northward freshwater transport is negative across A25 (northward salt transport) and largely takes place in the upper 500 m (or, in density space, in the top 14 layers, down to those containing the upper LSW), while the southward freshwater transport across OFLW is positive and of larger magnitude (Fig. 10).

As described in Appendix 1, the freshwater transport can be decomposed into the section averaged transport of averaged freshwater, the freshwater transport associated with the MOC, and that associated with the horizontal gyre circulation. Table 1 indicates that the mean freshwater transport across section A25 is dominated by the MOC component, but its variability (as described by the standard deviation) is dominated by the gyre component. Across section OFLW, the net transport is larger, and its variability smaller. If OFLW is considered as a single section (instead of 3), this primarily reflects the lower mean salinity of the mean southward flow across the Denmark Strait. In individual sections, however, the balance differs. The section averaged freshwater transport dominates the DSO and the Faeroe-Scotland Overflow, while the MOC component plays a smaller role and is only dominant in the Island-Faeroe Overflow.

There is a net freshwater transport convergence of 46 mSV between the two sections. Together with the freshwater fluxes at the surface, it contributes to changing the freshwater storage in the domain. The freshwater storage was calculated for each month and its yearly changes estimated by the difference between successive Januaries (Fig. 11). For the period 1963 to 2003, the mean increase in freshwater storage is 8 mSv. Hence, by a residual calculation, the mean freshwater flux across the air-sea interface and the lateral boundaries is 8 – 46 = - 38 mSV.

As precipitation exceeds evaporation in the subpolar gyre (e.g., Peterson et al. 2006) and sea ice melting and run-off increase the freshwater content, the surface salinity

restoring must be responsible for the negative mean residual freshwater flux, providing indeed – 77 mSv. The net effect of the other boundary fluxes (precipitation minus evaporation, ice melting, run-off, and horizontal mixing) is positive as expected, averaging to – 38 + 77 = 39 mSv. It is disturbing that the salinity restoring, which corrects for model and forcing biases, is the largest term in the mean freshwater budget.

A key question is whether the salinity restoring also dominates the salinity fluctuations, or it only has a small impact, as suggested in Hátún et al. (2005a) and MHS. An answer is provided by comparing the yearly fluctuations of the different terms of the freshwater budget between section A25 and OFLW (Fig. 11). The changes in freshwater content are dominated by the upper 500 m of the water column, and are highly correlated with the freshwater transport convergence. Both exhibit substantial standard deviations (σ = 57mSv and 39 mSv, respectively). To the residual freshwater flux variability (σ = 38 mSv), the physical boundary fluxes (σ = 30 mSv) and salinity restoring that damps the salinity fluctuations (σ = 28 mSv) contribute about equally. These terms are not independent. The freshwater transport convergence and the physical boundary fluxes are positively correlated, and they are anti-correlated with salinity restoring, in particular when the latter follows by 1 year, consistent with their forcing or damping role.

Although it cannot be stated (as in MHS) that the restoring does not dampen hydrographic anomalies, it accounts for approximately one-fourth of the variance in interannual to decadal changes in the freshwater content, which are largely controlled by the freshwater transport convergence and other boundary fluxes. Hence, on the time scales resolved by the simulation, the large-scale salinity changes are not too strongly affected by the surface restoring and their link with the MOC can be investigated with some confidence.

5. Link between salinity, the NAO, and ocean circulation in the eastern subpolar region

The relationship between interannual variations of salinity, the NAO and the circulation in the subpolar gyre was next investigated. Yearly salinity anomalies averaged over 500 m-thick layers in the two eastern subpolar domains, IRM and ENA, were shown in Fig. 7. Precipitation increases during positive NAO phases (Bojariu and Reverdin 2002), and the upper layer salinity are significantly anti-correlated with the NAO index in both domains. However, as illustrated for the Irminger Sea (Fig. 12, top left), the maximum anti-

correlation occurs in the two domains when the NAO leads by 1 year. A similar lag was also found by MHS for the whole subpolar gyre. Since surface freshwater exchanges should exhibit maximum anti-correlation with the near-surface salinity at zero lag when using yearly data (Mignot and Frankignoul 2004), the negative correlation at lag-1 suggests an additional influence from salinity advection. The salinity anomalies in the 500-1000 m layer behave similarly, but tend to slightly lag those in the layer above since some additional time is required to vertically mix the anomalies downward.

An advective influence is confirmed by considering the horizontal freshwater transport. To do so, we consider the larger eastern subpolar domain (IRM+ENA) of section 4. Across the southern section A25, the northward freshwater transport, whose variability is dominated by the gyre component (Table 1), is positively correlated with the NAO (Fig.13, top, plain line). This largely reflects the freshwater transport associated with BTSF EOF2, the anticyclonic intergyre gyre rapidly forced by the NAO wind stress (section 2), which reduces the net southward freshwater transport (northward salt transport) by the mean circulation in a positive NAO phase. This is seen in the regression of the northward freshwater transport on BTSF PC2, which is positive except along Greenland and near 20°W (Fig.14), yielding a net freshwater transport of 20 mSv. A northward freshwater transport is also associated with BTSF EOF1, but it is slightly smaller (14 mSv).

It may seem surprising that the northward freshwater transport does not decrease 2 years after a positive NAO phase when the MOC has become stronger, since more salt is transported northward when the MOC intensifies (Fig. 13, middle panel). However, the northward salt transport associated with MOC PC1 is cancelled by the increased northward freshwater transport associated with the intensification of the subpolar gyre, as represented by BTSF PC1 (Fig. 13, lower panel). During this intensification, the subpolar front eastward exhibits an eastward shift (discussed in section 3), thus reducing the northward advection of saline subtropical waters into the subpolar domain. Hence, the in-phase variation of the MOC and the subpolar gyre circulation prevents the MOC from significantly modulating the northward freshwater transport on the time scales resolved by the hindcast. Such cancellation does not take place in the climate models where the MOC and the gyre circulation do not intensify in phase. Finally, note in Fig. 13 (bottom) that the gyre component of the freshwater transport across A25 also leads BTSF PC1 by 2 yr. This simply reflects that the increased freshwater transport by the NAO driven intergyre gyre (see above) is slightly larger and occurs about two years before that by the NAO-driven intensification of the subpolar gyre (BTSF PC2 leads BTSF PC1 by 2 years).

In summary, precipitation increases over the eastern subpolar domain in a positive NAO phase while the wind-driven intergyre gyre enhances the freshwater influx from the southern boundary, with practically no time lag. After a delay of about 2 years, both the MOC and the subpolar gyre circulation intensify, but they affect the northward freshwater flux into the domain in an opposite way and thus have little net effect. As documented by MHS, the southward freshwater transport across OFLW varies primarily in phase with the NAO, reflecting increasing inflows of saline North Atlantic Water to the Nordic Seas and outflows of fresh Polar Water in a positive NAO phase. Hence, the variability of the net freshwater transport convergence between the two sections is even more positively correlated with the NAO (Fig. 13, top, dashed line).

Figure 12 (middle) shows that the salinity anomalies in the Irminger Sea are strongly anti-correlated with IRMi, the deep convection index (from Fig 3). This is consistent with the positive correlation between the NAO and IRMi at lag 0 and 1 (DF08), and the anti-correlation above. Considering salinity in a smaller domain around the deep convection site does not significantly alter this result. Moreover, DFD showed that since fresh surface water inhibits convection, convection in the Irminger Sea is thermally driven. Although this anti-correlation could also imply that Irminger Sea convection produces relatively fresh Labrador Sea Water, in either case, salinity served as a passive tracer, a point that was established by MHS. Correspondingly, salinity is slightly anti-correlated with MOC PC1, our index of the MOC (Fig. 12, bottom). Anti-correlation also exists between the salinity anomalies and BTSF PC1. Here, salinity leads by 0 - 1 yr in the upper layer (but significance is marginal) and lags by 0 - 2 yr at greater depth.

In the Labrador Sea region, we found no significant correlations between upper layer salinity and deep convection, which is driven by surface heat fluxes (FDC), consistent with the observations discussed by Lazier et al. (2002). Neither was there any direct link between salinity and MOC PC1 or BTSF PC1. However, this may be affected by the strong underestimation in the model of the freshwater pulse from the Arctic during the GSA. As a whole, these findings are broadly consistent with MHS, who found that the peaks of freshwater content in the upper 1000 m of the entire subpolar gyre preceded peaks in gyre strength or width by about 1 year.

These relationships diagnosed for the freshwater transport convergence, deep convection in the Irminger Sea, BTSF PC1, and MOC PC1 lead us to assert that salinity played a passive role in the subpolar gyre circulation variability of the last 4 decades. Changes in freshwater convergence into the subpolar domain were mostly controlled by

NAO-driven advection – through variable inflows from the subtropics and Nordic Seas. In the hindcast, surface fluxes of freshwater and ice melting played a comparatively lesser role, although this evaluation depends on the accuracy of the NCEP forcing fields. The contribution to salinity variability from restoring in the simulation was also considerably smaller than advection and other boundary fluxes.

6 Summary and discussion

We have used an OGCM forced by fluxes derived from the NCEP reanalysis to investigate linkages between salinity and interannual to decadal changes of the North Atlantic circulation. The focus was on the subpolar region since the MOC variability in the model is primarily driven by changes in deep water formation in the Irminger Sea and, to a lesser extent, the Labrador Sea. The simulation had been shown to reproduce fairly well the evolution of many hydrographic features and the weakening of the subpolar gyre since the mid 90s (Hátún et al. 2005, MHS). Here, a further evaluation of the time evolution of observed and simulated salinity fields was performed through direct comparisons with the available record of hydrographic measurements using Hydrobase (Curry 2002). It indicates that the amplitude changes of simulated salinity distributions in the upper layers are consonant in the Irminger Sea (0-1500m) and the eastern North Atlantic (0-500m) with the observed changes from the mid-1960s onward, although the magnitude of the freshwater influx during the GSA of the early 1970s is slightly underestimated, presumably due to a strong underestimation of the freshwater and sea ice pulse from the Arctic that contributed to the GSA in the Labrador Sea during the late 1960s. The salinity restoring to an observed SSS climatology inhibited some of the SSS variations, but overall it accounts for approximately 25% of the variance of the interannual to decadal changes in the freshwater content, which are thus mostly controlled by the freshwater transport convergence and other boundary fluxes. This justifies using the model to investigate linkages between salinity, the NAO, and the ocean circulation in the eastern subpolar region for the period 1963-2003, when the watermasses in the regional model seem to have adjusted to the time-varying forcing.

In the hindcast, the interannual to decadal variability of salinity in the eastern subpolar region is largely driven by the freshwater transport convergence associated with horizontal circulation changes, although surface freshwater fluxes also contribute substantially. The NAO plays an important role. A high NAO increases precipitation and rapidly reduces the

northward salt transport from the south via the wind driven anticyclonic intergyre gyre, while more freshwater flows southward across the Greenland-Scotland ridge. Since the NAO is a main driver of convection in the Irminger Sea, fresher water is found near the sinking region during convective events. Salinity also serves as a passive tracer in the Labrador Sea. Our analysis supports and complements MHS, who focused more on the freshwater exchanges between the subpolar gyre and the Nordic seas.

As discussed in DF08, the low-frequency variability of the simulated MOC is mostly driven by the surface heat exchanges and the wind forcing associated with the NAO. The intensification of the MOC that follows a positive NAO phase by about 2 years does not lead to an increase in the northward salt transport into the subpolar domain because it is cancelled by the concomitant intensification of the subpolar gyre which shifts the subpolar front eastward and reduces the northward salt transport by the NAC waters. The fact that the MOC and the subpolar gyre circulation varied largely in phase at low frequency thus prevented significant modulation of the northward freshwater transport into the subpolar region and contributed to the passive role of salinity in the last 4-5 decades.

Whether salinity is active or passive has seldom been discussed in other OGCM hindcasts. Häkkinen (2002) found (with no salinity restoring) that sea ice export through the Denmark Strait could have an important impact on the Labrador Sea SSS at interannual timescales, but little influence on deep convection, and that SSS was mainly a passive tracer of the circulation changes at decadal scales. Haak et al. (2003) found (with very little salinity restoring) that even the large salinity changes associated with GSA had little lasting impact on the MOC. Hence, these OGCM hindcasts are consistent with the passive salinity role found here and in MHS. The observed changes in the freshwater content of the Subpolar Basins (Curry and Mauritzen 2005, Peterson et al. 2006) would also suggest that salinity is passive in the subpolar domain if the simulated MOC changes were realistic, which is an admittedly arguable assumption.

This drastically differs from the active role that salinity plays in most coupled models (section 1). Are the differences generic, have they to do with timescale, or do they reflect an unusual evolution of the salinity fields in the second half of the 20th century?

Although the present hindcast has limitations, it presents a MOC evolution that is broadly similar to that found in several other models, including some without salinity restoring (Eden and Young 2001, Bentsen et al. 2004) or freshwater flux forcing (Böning et al. 2006). The simulated decrease of the MOC since the mid 90s was also reproduced in the global synthesis (OGCM with data assimilation and no restoring) of Kohl et al. (2007).

Admittedly, the underestimation of the dense water flow across the Greenland-Scotland ridge in the present hindcast limited the influence of the Nordic Seas. However, Latif et al. (2006) suggested that the role of the overflows is expected to be small in present day conditions, based on sensitivity experiments with two different OGCMs.

The other hindcasts similarly show that the intensification of the MOC occurs broadly in phase with that of the subpolar gyre (e.g., Eden and Willebrand 2001, de Coëtlogon et al. 2006, Böning et al. 2006). Hence, the present simulation seems broadly representative of OGCM simulations, and a key to the differences with the coupled models is the different lead-lag relation between gyre strength and MOC. In the coupled models, the intensification of the subpolar gyre precedes that of the MOC by several years (for instance, 6 years in HadCM3, Dong and Sutton 2005). Hence, there is no cancellation between MOC and gyre northward freshwater transport, and a stronger MOC brings more warm saline waters in the subpolar domain, which subsequently enhances the MOC.

However, inaccurate forcing data and a lack of knowledge of the initial conditions are main sources of uncertainty in OGCM hindcasts. Ensemble simulations with different initial conditions in Bentsen et al. (2004) suggest that there is a 5-10 yr adjustment time for the North Atlantic MOC plus a much longer one that mainly causes a small off-set between each hindcast, but with little effect on the MOC variations. In Haak et al. (2003), the dispersion of the simulations can be large, yet without obscuring the mean MOC changes. Hence, the initial conditions likely contributed to the lack of resemblance with the observed salinity changes during the first 15 years or so of the run, but they are unlikely to have strongly contaminated the upper subpolar region during the 1963-2003 period that forms the basis of our analysis. This would be consistent with the agreement in the overlapping period between the simulated MOC changes and those in the longer simulation (albeit solely forced by the NAO and with restoring at 70°N) of Eden and Young (2001).

Another possible cause of the differences with the coupled models is that salinity could only become active on longer timescales than can be resolved by 50-yr OGCM hindcasts. Indeed, the Atlantic MOC may behave differently on multidecadal and centennial timescales, as suggested by the longer lag with the NAO forcing in the simulation of Eden and Young (2001), by the strong influence of freshwater exchanges with the Arctic in multidecadal to centennial MOC fluctuations (Delworth et al 1993, Vellinga and Wood 2004, Jungclaus et al. 2005), or by the dominant influence of large salinity changes in the Nordic Seas found by Schweckendiek and Willebrand (2005) in global warming conditions. Yet, salinity was also active at periods of about 25-yr in HadCM3 (Dong and Sutton 2005)

and 15-20 yr in IPSL-CM4 (Msadek and Frankignoul, 2008), timescales that should be well represented by the hindcast.

Finally, it could also be that coupled models lock into unrealistic modes of variability because of their often limited resolution, their biased climatology and, in particular, generally ill-placed convective zones and poor mean current locations in the North Atlantic, which may lead to an overestimation of salinity advection into the sinking regions.

More observations, a more thorough investigation of the freshwater balance in coupled models, more realistic hindcasts with improved freshwater forcing and mixing processes, and high resolution oceanic reanalyses are needed to determine why coupled models and hindcasts seem to behave differently.

Appendix 1

The freshwater transport across a section can be decomposed into components linked to the different kinds of oceanic circulation. The section-averaged transport of averaged freshwater content is given by

$$<\underline{F}>(t)\ <\underline{v}>(t) \int\int dx\ dz,$$

and the freshwater transport associated with the MOC by

$$\int <F>(z,t)\ <v>(z,t)\ dz \int dx,$$

where $<\underline{f}>$ denotes the section average of a variable f and $<f>(z) = \int (f(x,z) - <\underline{f}>)dx$ its zonally averaged deviation. The residual is the freshwater transport associated with the gyre circulation (plus the small contribution of horizontal and eddy mixing). The calculation is made with monthly anomalies, but we consider yearly averages.

Acknowledgments

We thank Helge Drange and Anne Britt Sandø for providing the OGCM data, and the reviewers for their pertinent and constructive comments. Support from NSF Grant 82677800 with the Woods Hole Oceanographic Institution, and (to CF) from the Institut universitaire de France and European FP6 project DYNAMITE (contract 003903-GOCE) and (to JD) from the NOAA Office of Hydrologic Development through a scientific appointment administered by UCAR is gratefully acknowledged.

References

Belkin IM, Levitus S, Antonov J, Malmberg SA (2003) « Great Salinity Anomalies » in the North Atlantic. Prog Oceanogr 41:1-68

Bentsen M, Drange H, Furevik T, Zhou T (2004) Simulated variability of the Atlantic meridional overturning circulation. Clim Dyn 22 : 701-720.

Bentsen M, Drange H (2000) Parameterizing surface fluxes in ocean models using the NCEP/NCAR reanalysis data. In RegClim General Technical Report 4, Norwegian Institute for Air Research, Kjeller, Norway, 149-158 pp.

Bersch M (2002) North Atlantic Oscillation-induced changes of the upper layer circulation in the northern North Atlantic Ocean. J Geophys Res 107(10), 3156, doi:10.1029/2001JC000901.

Bleck R, Rooth C, Hu D, Smith LT (1992) Salinity-driven thermocline transients in a wind- and thermohaline-forced isopycnic coordinate model of the North Atlantic. J Phys Oceanogr 22:1486-1505

Bojariu R, Reverdin G (2002) Large-scale variability modes of freshwater flux and precipitation over the Atlantic. Clim Dyn 18: 369-381

Böning CW, Scheinert M, Dengg J, Biastoch A, Funk A (2006) Decadal variability of subpolar gyre transport and its reverberation in the North Atlantic overturning. Geophys Res Lett 32: doi:10.1029/2006GL026906

Boyer T, Levitus S, Antonov J, Locarnini R, Mishonov A, Garcia H, Josey SA (2007) Changes in freshwater content in the North Atlantic Ocean. Geophys Res Lett 34:doi:10.1029/2007GL030126

Bryan F, Danabasglu G, Nakashiki N, Yoshida Y, Kim DH, Tsutsui J (2006) (2006) Response of the North Atlantic thermohaline circulation and ventilation to increasing carbon dioxide in CCSM3. J Climate 19: 2382-2397

Cuny J, Rhines PB, Lazier J (2005) Convection above the Labrador continental slope. J Phys Oceanogr 35: 489-511

Curry RG (2002) Hydrobase 2: A Database of Hydrographic Profiles and Tools for Climatological Analysis "http://www.whoi.edu/science/PO/hydrobase", Woods Hole Oceanographic Institution

Curry RG, McCartney MS (2001) Ocean gyre circulation changes associated with the North Atlantic Oscillation. J Phys Oceanogr 31: 3374-3400

Curry R, Dickson R, Yashayaev I (2003) A change in the freshwater balance of the Atlantic Ocean over the past four decades. Nature 426: 826-829.

Curry RG, Mauritzen C (2005) Dilution of the northern North Atlantic ocean in recent decades. Science 308: 1772-1774.

de Coëtlogon G, Frankignoul C, Bentsen M, Delon C, Haak H, Massina S, Pardaens A (2006) Gulf Stream variability in five oceanic general circulation models. J Phys Oceanogr 36: 2119-2135

Delworth T, Greatbatch RJ (2000) Multidecadal thermohaline circulation variability driven by atmospheric surface flux forcing. J Clim 13: 1481-1495.

Delworth T, Manabe S, Stouffer R (1993) Interdecadal variations of the thermohaline circulation in a coupled ocean-atmosphere model. J Clim 6: 1993-2011.

Delworth T, Manabe S, Stouffer R (1997) Multidecadal climate variability in the Greenland Sea and surrounding regions: A coupled model simulation. Geophys Res Lett 24: 257-260.

Deshayes J, Frankignoul C, Drange H (2007) Formation and export of deep water in the Labrador and Irminger Seas in a GCM. Deep-Sea Res 54: 510-532

Deshayes J, Frankignoul C (2008) Simulated variability of the circulation in the North Atlantic from 1953 to 2003. J Clim 21: 4919-4933

Dickson RR, Brown J (1994) The production of North Atlantic Deep Water, sources, rates, and pathways. J Geophys Res 99:12,319-12,341

Dickson RR, Meincke J, Malmberg SA, Lee AJ (1988) The "Great Salinity Anomaly" in the northern North Atlantic, 1968-1982. Progr Oceanogr 20: 103-151.

Dickson RR, Yashayaev I, Meincke J, Turrel JB, Dye S, Holfort J (2002) Rapid freshening of the deep North Atlantic ocean over the past four decades. Nature 146: 832-837.

Dong B, Sutton RT (2005) Mechanisms of interdecadal thermohaline circulation variability in a coupled ocean-atmosphere GCM. J Clim 18: 1117-1135.

Eden C, Willebrand J (2001) Mechanism of interannual to decadal variability of the North Atlantic Circulation. J Clim 14: 2266-2280.

Eden C, Young T (2001) North Atlantic interdecadal variability: oceanic response to the North Atlantic Oscillation (1865-1997). J Clim 14: 676-691

Eldevik T (2002) On frontal dynamics in two model oceans. J Phys Oceanogr 32 :2915-2925

Falina A, Sarafanov A, Sokov A (2007) Variability and renewal of Labrador Sea Water in the Irminger basin in 1991-2004. J Geophys Res 112: C01006, doi:10.1029/2005JC003348

Flatau MK, Talley LD, Niiler PP (2003) The North Atlantic Oscillation, surface current velocities and SST changes in the subpolar North Atlantic. J Phys Oceanogr 19:2355-2369

Ganachaud A, Wunsch C (2000) Improved estimates of global ocean circulation, heat transport and mixing from hydrographic data. Nature 408:453-456

Haak H, Jungclaus J, Mikolajewicz U, Latif M (2003) Formation and propagation of great salinity anomalies. Geophys Res Lett 30: 1473, doi:10.1029/2003GL017065

Häkkinen S (1999) A simulation of thermohaline effects of a great salinity anomaly. J Clim 12: 1781-1795

Häkkinen S (2002) Surface salinity variability in the northern North Atlantic during recent decades. J Geophys Res 107: 8003, doi:10.1029/2001JC000812

Häkkinen S, Rhines PB (2004) Decline of subpolar North Atlantic circulation during the 1990s. Science 309: 555-559

Hátún H, Sandø AB, Drange H, Hansen B, Valdimarsson H (2005a) Influence of the Atlantic Subpolar Gyre on the thermohaline circulation. Science 309:1841-1844.

Hátún H, Sandø AB, Drange H, Bentsen M (2005b) Seasonal to decadal temperature variations in the Faroe-Shetland inflow waters. The Nordic Seas: An Integrated Perspective. H. Drange, T. M. Dokken, T. Furevik, R. Gerdes and W. Berger, American Geophysical Union, 158, 239-250.

Hawkins E, Sutton R (2007) Variability of the Atlantic thermohaline circulation described by three-dimensional empirical orthogonal functions. Clim Dyn 29:745-762

Josey SA, Marsh R (2005) Surface freshwater flux variability and recent freshening of the North Atlantic in the eastern subpolar gyre. J Geophys Res 110, C05008, doi:10.1029/2004JC002521

Jungclaus J, Haak H, Latif M, Mikolajewicz U (2005) Arctic-North Atlantic interactions and multidecadal variability of the meridional overturning circulation. J Clim 18: 4013-4031.

Kalnay E, Coauthors (1996) The NCEP/NCAR Reanalysis Project. Bull Amer Meteor Soc 77: 437-471

Kohl A, Stammer D, Cornuelle B (2007) Interannual to decadal changes in the ECCO global synthesis. J Phys Oceanogr 37: 313-337

Lavender KL, Davis RE, Owens WB (2000) Mid-depth recirculation observed in the interior Labrador and Irminger Seas by direct velocity measurements. Nature 407: 66-69.

Latif M, Böning C, Willebrand J, Biastoch A, Dengg J, Keenlyside N, Schweckendiek U (2006) Is the thermohaline circulation changing? J Climate 18: 4631-4637

Lazier J, Hendry R, Clarke A, Yashayaev I, Rhines P (2002) Convection and restratification in the Labrador Sea, 1990-2000. Deep-Sea Res I 49: 1819-1835

Lumpkin R, Speer K (2003) Large-scale vertical and horizontal circulation in the North Atlantic ocean. J Clim 33: 1902-1920

Levitus S, Boyer TP (1994) World Ocean Atlas 1994 Volume 4: Temperature. NOAA Atlas NESDIS 4.

Levitus S, Burgett R, Boyer TP (1994) World Ocean Atlas 1994 Volume 3: Salinity. NOAA Atlas NESDIS 3.

Mauritzen C, Hjøllo SS, Sandø AB (2006) Passive tracers and active dynamics: a model study of hydrography and circulation in the northern North Atlantic. J Geophys Res 111: C08014, doi:10.1029/2005JC003252

Mignot J, Frankignoul C (2004) Interannual to interdecadal variability of sea surface salinity in the Atlantic and its link to the atmosphere in a coupled model. J Geophys Res 109: C04005

Msadek R, Frankignoul C (2008) Atlantic multidecadal oceanic variability and its influence on the atmosphere in a climate model. Clim Dyn, DOI 10.1007/s00382-008-0452-0

Peterson BJ, McClelland J, Curry R, Homes RM, Walsh JE, Agaard K (2006) Trajectory shifts in the Arctic and subarctic freshwater cycle. Science 313: 1061-1066.

Pickart RS, Straneo F, Moore GWK (2003) Is Labrador Sea Water formed in the Irminger basin ? Deep-Sea Res Part 1 50: 23-52.

Reverdin G, Niiler PP, Valdimarsson H (2003) North Atlantic ocean surface currents. J Geophys Res 108, doi:10.1029/2001JC001020

Rhein M, Fischer J, Smethie WM, Smythe-Wright D, Weiss RF, Mertens C, Min DH, Fleischmann U, Putka A (2002) Labrador Sea Water: Pathways, CFC inventory and formation rates. J Phys Oceanogr 32:648-665

Rousset C, Houssais MN, Chassignet E (2007) A multi-model study of the restratification phase in an idealized convection basin. Ocean Dyn, submitted.

Schweckendiek U, Willebrand J (2005) Mechanisms affecting the overturning response in global warming simulations. J Clim 18: 4925-4936

Vellinga M, Wood RA (2002) Global climatic impacts of a collapse of the Atlantic thermohaline circulation. Climatic change 54: 251-267

Vellinga M, Wu P (2004) Low-latitude freshwater influence on centennial variability of the Atlantic thermohaline circulation. J Clim 17:4498-4511

Willebrand J. and Coauthors (2001) Circulation characteristics in three eddy-permitting models of the North Atlantic. Progress in Oceanogr 48: 123-161

Wu P, Wood R, Stott P (2004) Does the recent freshening trend in the North Atlantic indicate a weakening of the thermohaline circulation? Geophys Res Lett 31: L02301, doi:10.1029/2003GL018584

Zhu X, Jungclaus J (2008) Interdecadal variability of the meridional overturning circulation as an ocean internal mode. Clim Dyn 31:731-741

Table 1

Freshwater transport	net	section averaged	overturning	gyre component
A25	−82 ±33	−4 ±2	−83 ±16	6 ±31
correlation with net freshwater transport		−0.22	0.44	0.95
3 overflows	−128 ±13	−0.15 ±0.78	7.1 ±1.4	−135 ±13
correlation with net freshwater transport		−0.36	0.12	0.99
DSO	−62 ±10	−46 ±8	10 ±1.4	−26 ±3
correlation with net freshwater transport		0.91	0.18	0.53
IFO	−20 ±3	−6.6 ±2.2	−1.3 ±0.66	−12 ±3
correlation with net freshwater transport		0.25	−0.48	0.72
FSO	−46 ±5	−31 ±5	−11 ±1.5	−3.5 ±0.6
correlation with net freshwater transport		0.94	0.53	0.80

Table 1: Mean and standard deviation of the annual freshwater transport (in mSv) across sections A25, OFLW, Denmark Strait (DSO), Iceland-Faeroe (IFO), and Faeroe-Scotland (FSO). The decomposition of freshwater transport was done on monthly data, and the correlations calculated after linear detrending of the time series.

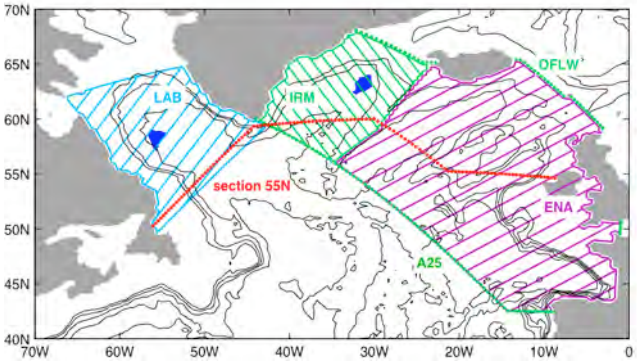

Fig. 1 Bathymetry of the model between 40°N and 70°N (contour interval 1000 m), location of the main areas of deep convection (blue), and domains or sections considered in the text.

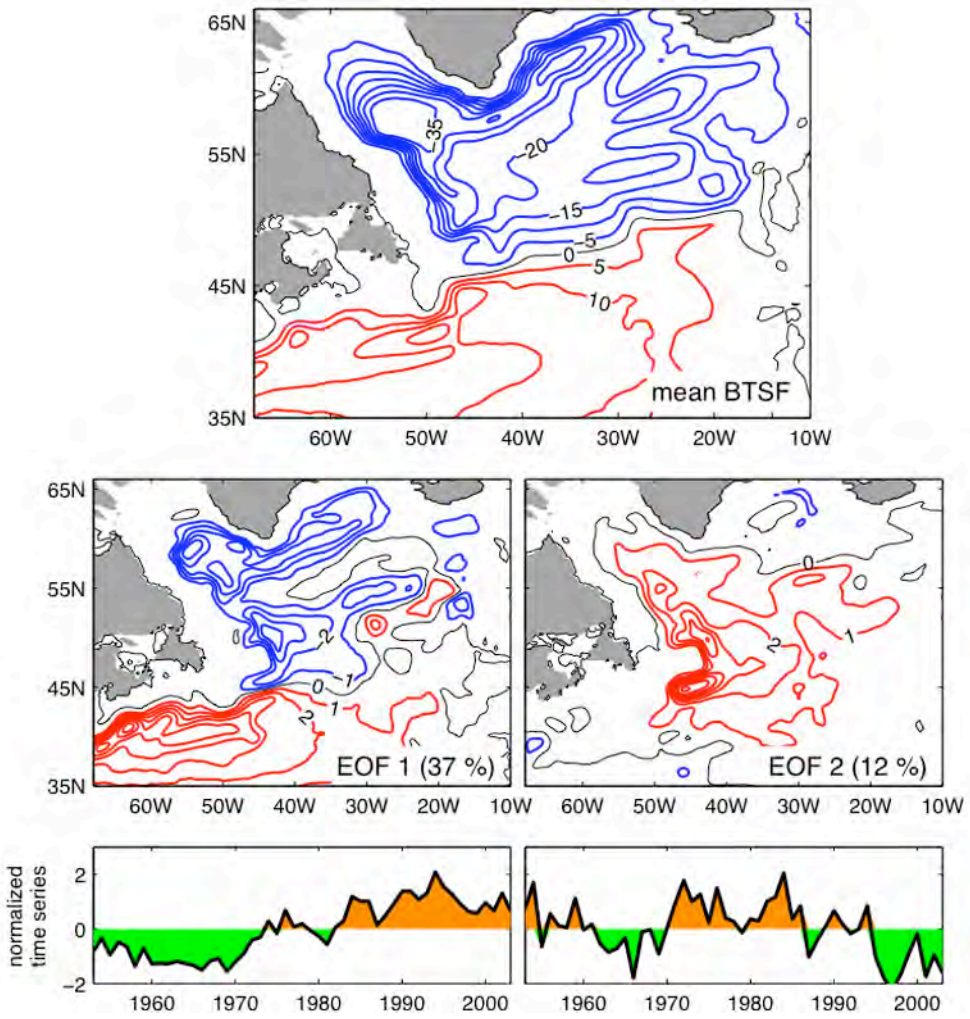

Fig. 2 Mean value (top) and first two rotated EOFs (10 modes were selected for the varimax rotation) (middle) and corresponding PCs (bottom) of the BTSF. The percentage of represented variance is indicated and the PCs are normalized so the EOFs give typical amplitudes. Contour interval is 1 Sv.

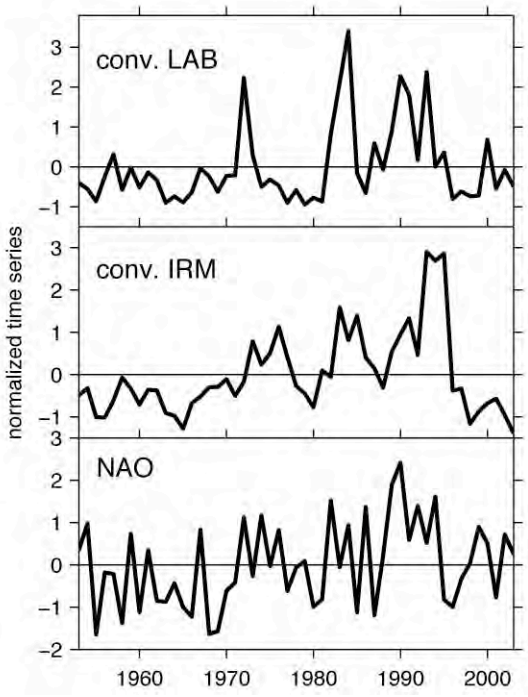

Fig. 3 Normalized time series of convection (defined as the mixed layer volume from February to April in the areas in Fig.1 in the Labrador (top) and Irminger (middle) Seas, and NAO index (defined here as the yearly time series of PC1 of the monthly sea level pressure anomalies in the North Atlantic, bottom).

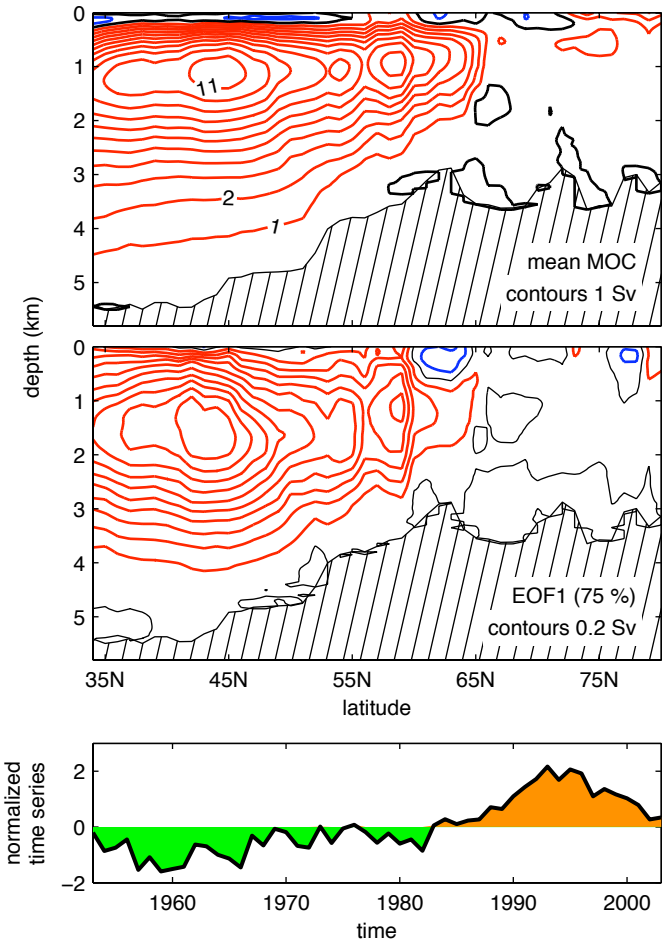

Fig. 4 Mean value *(top)*, first rotated EOF (10 modes were selected for the varimax rotation) *(middle)* and corresponding PC *(bottom)* of the MOC. The percentage of represented variance is indicated and the PC is normalized so the EOF gives the typical amplitude. Contour interval is 0.2 Sv.

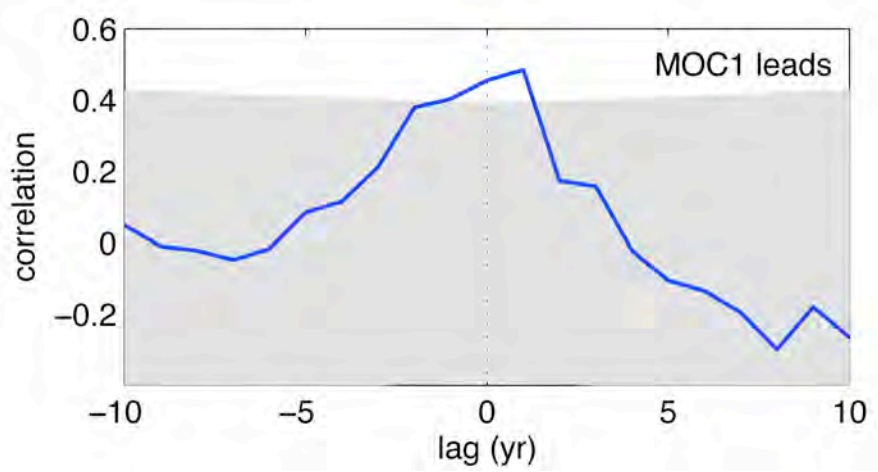

Fig. 5 Cross-correlation between MOC PC1 and BTSF PC1. The shaded area indicates the 90 % confidence interval. MOC PC1 leads at positive lags.

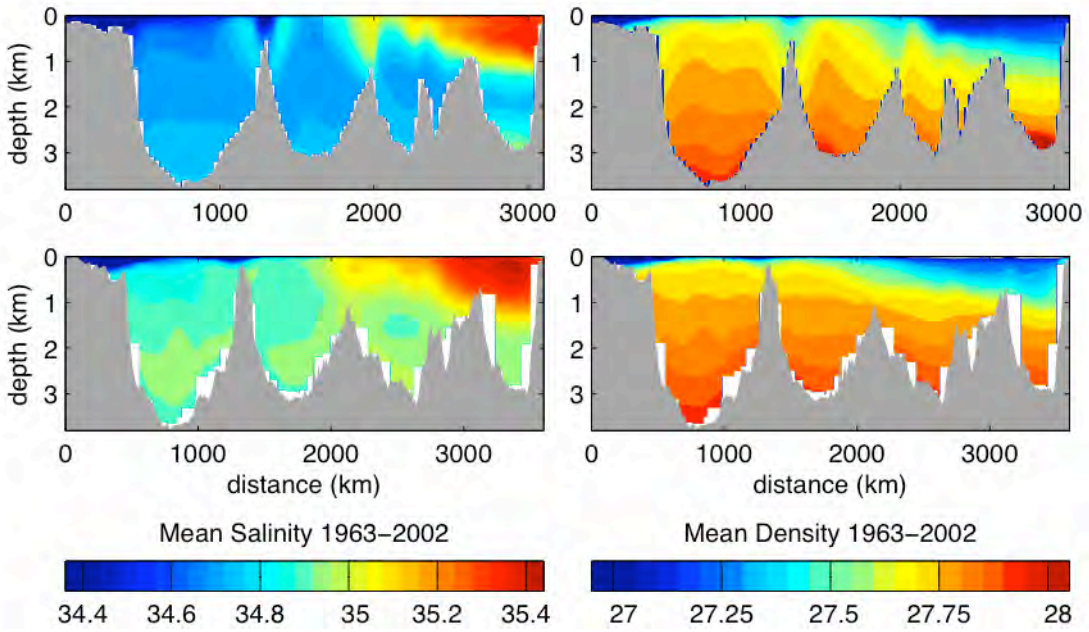

Fig. 6 1963-2002 mean salinity *(left)* and potential density *(right)* distribution along the 55°N section for *(top)* the model and *(bottom)* the observations (from HydroBase).

.

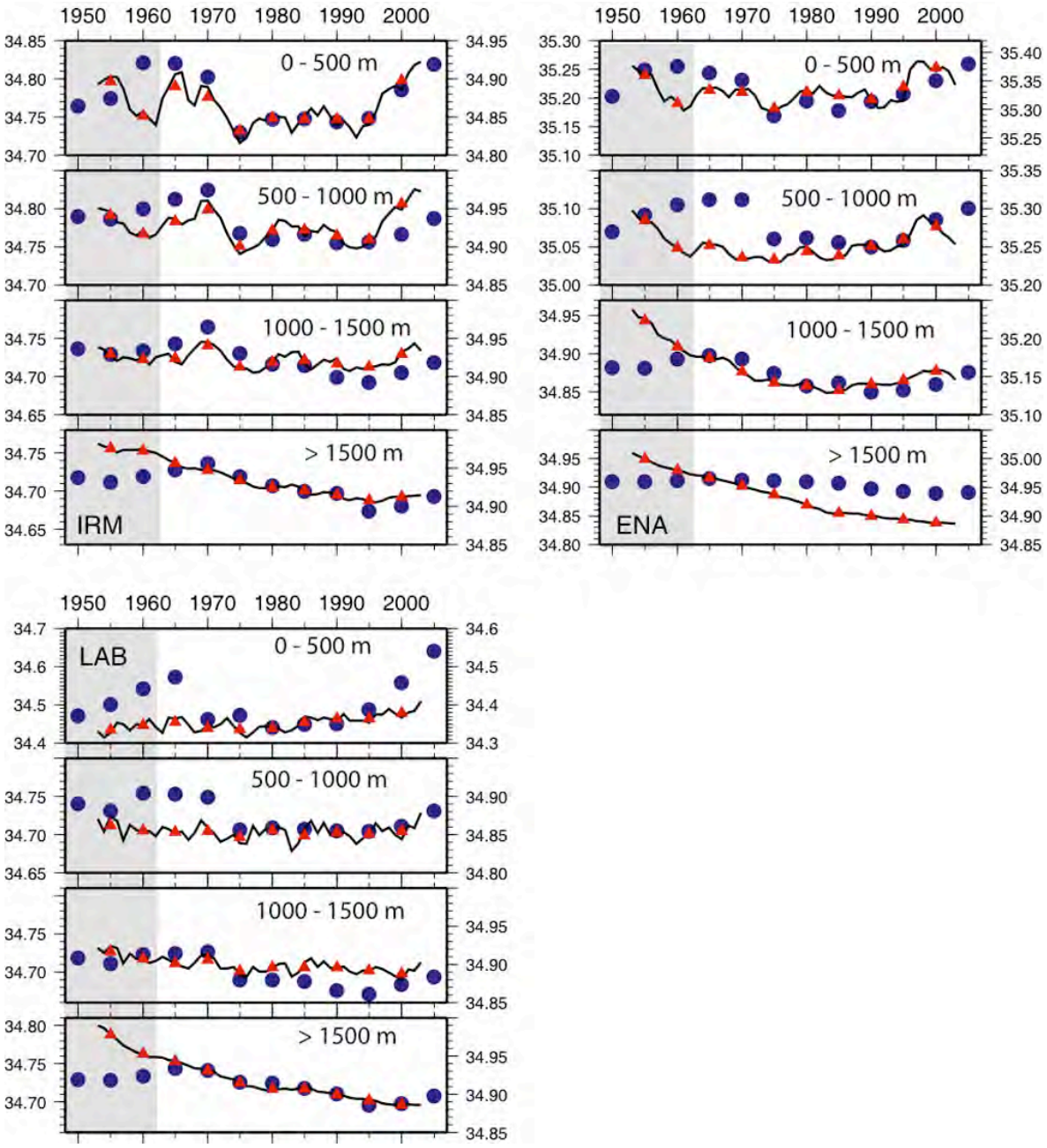

Fig. 7 Timeseries of layer-averaged salinity for three regions (locations shown in Fig 1): IRM (Irminger Basin, *top left*), ENA (Eastern North Atlantic, *top right*), and LAB (Labrador Basin, *bottom*). Layer-averaged salinity was computed for 5-year time periods from observations (blue circles, right axes) and simulations (red triangles, left axes). Black curves are annual salinities from the simulation. Depth ranges of layers are denoted in each

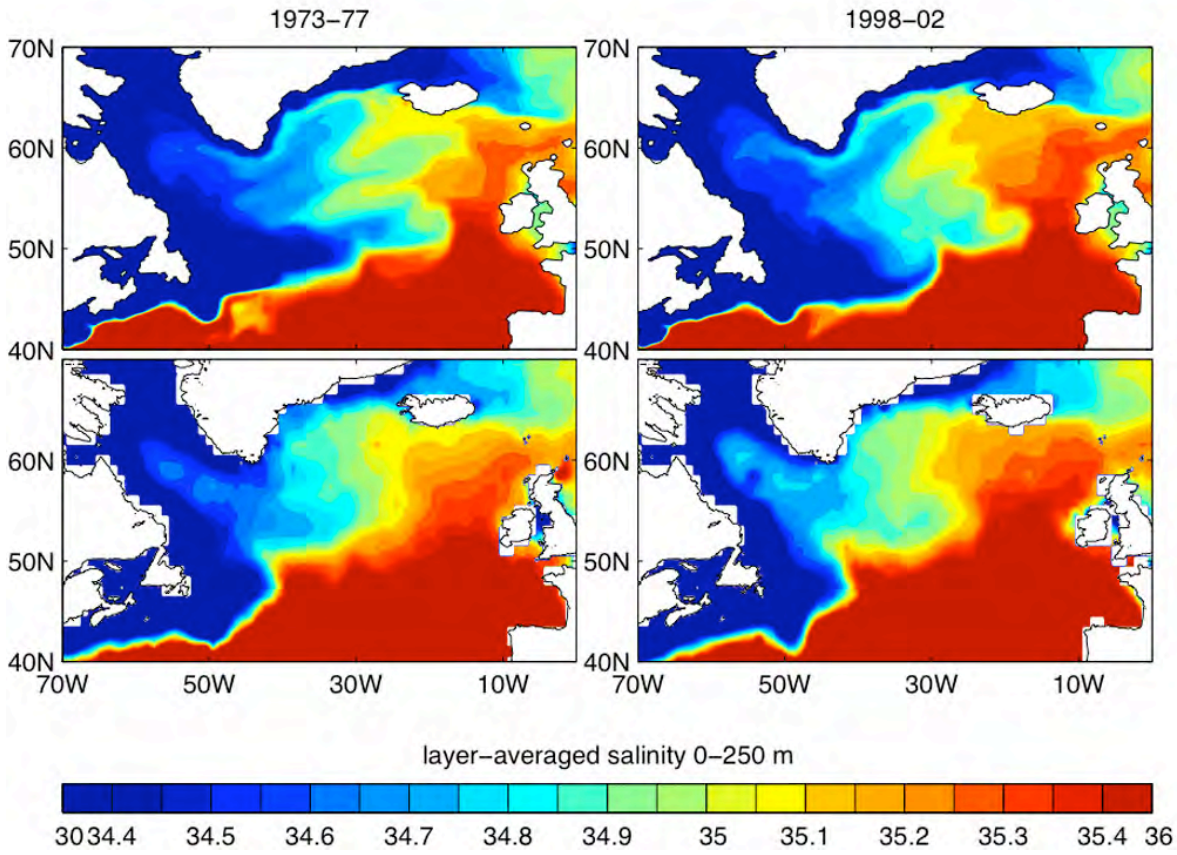

Fig. 8 Salinity in the 0-250 m layer in 1973-77 *(left)* and 1998-2002 *(right)* for the model *(top)* and the observations *(bottom)*

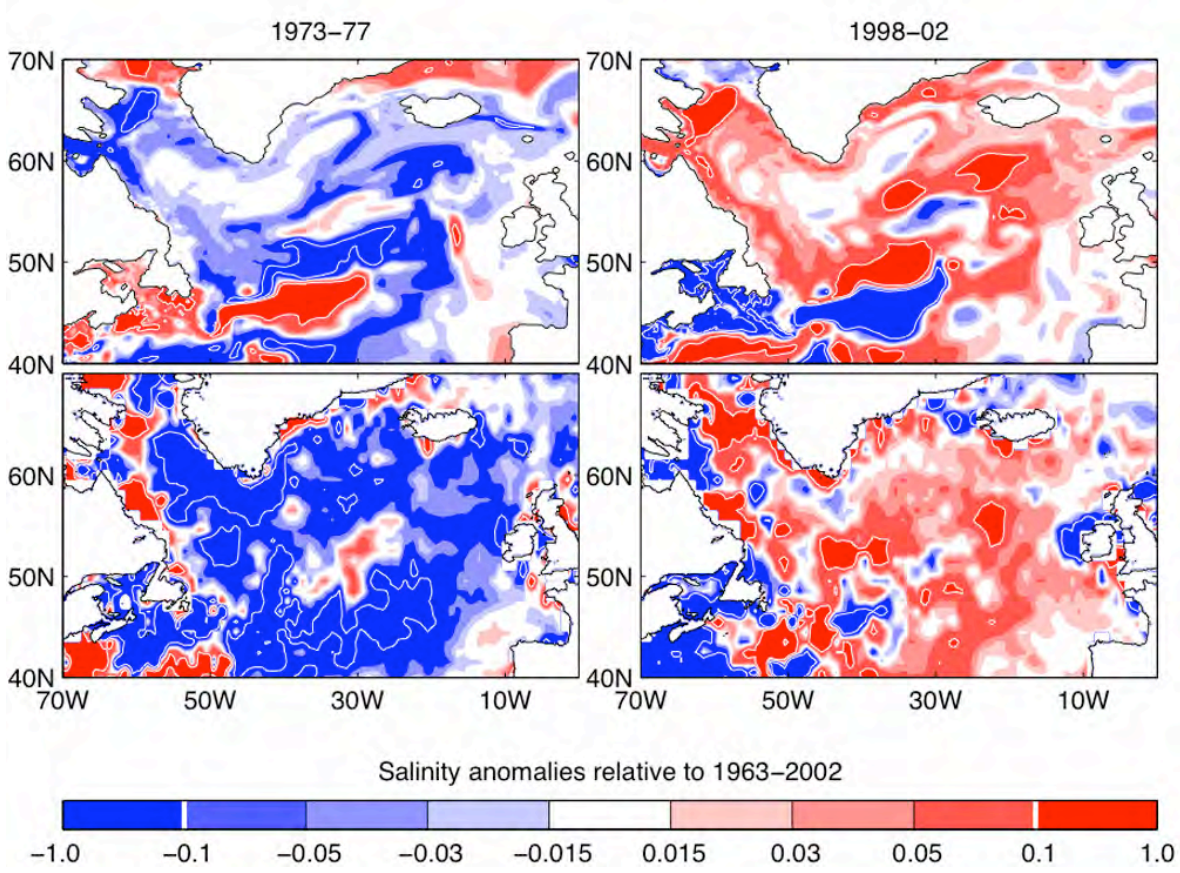

Fig. 9 Simulated *(top)* and observed *(bottom)* salinity anomaly for 1973-1977 *(left)* and 1998-2002 *(right)*.

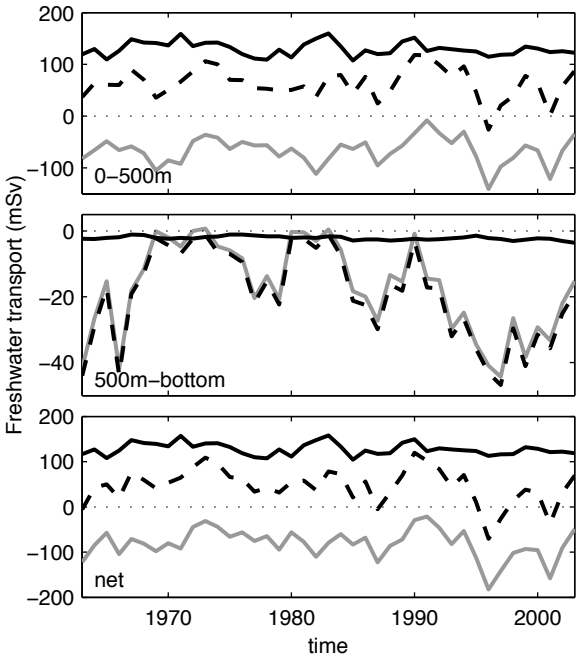

Fig.10 Transport of freshwater across section A25 (grey, positive northward), OFWL (black, positive southward), and net freshwater convergence between the two sections and the Channel one (dashed) as a function of time for the layer 0 – 500 m *(top)*, 500 – 1000 m *(middle)* and for the whole water column *(bottom)*.

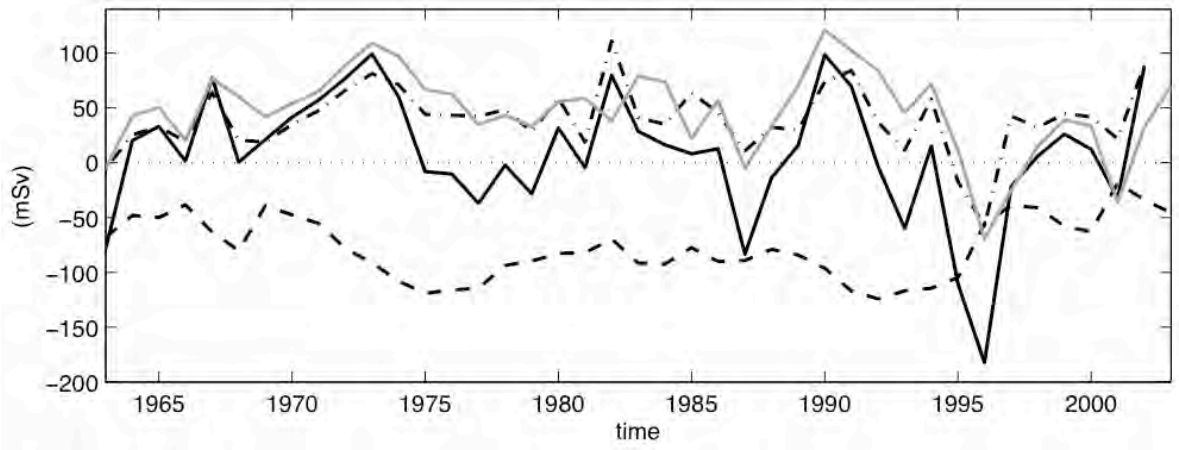

Fig. 11 Time series of the rate of change of the freshwater content (continuous line), the freshwater flux convergence (grey line), the salinity restoring flux (dotted line), and the other boundary fluxes (dashed-dotted line) in the eastern subpolar gyre. Units are mSv.

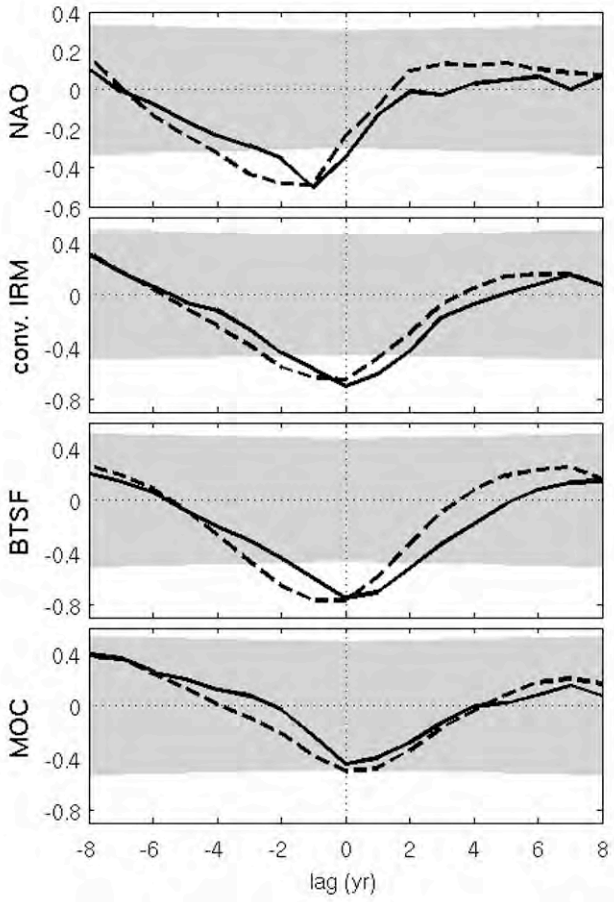

Fig. 12 Cross-correlation of the salinity in IRM in the 0-500 m (continuous line) and 500-1000 m (dashed line) layer with the NAO *(top)*, deep convection in the Irminger Sea *(middle)*, and the two circulation indices *(bottom panels)*. Salinity leads at positive lags. The shaded area indicates the 90 % confidence interval.

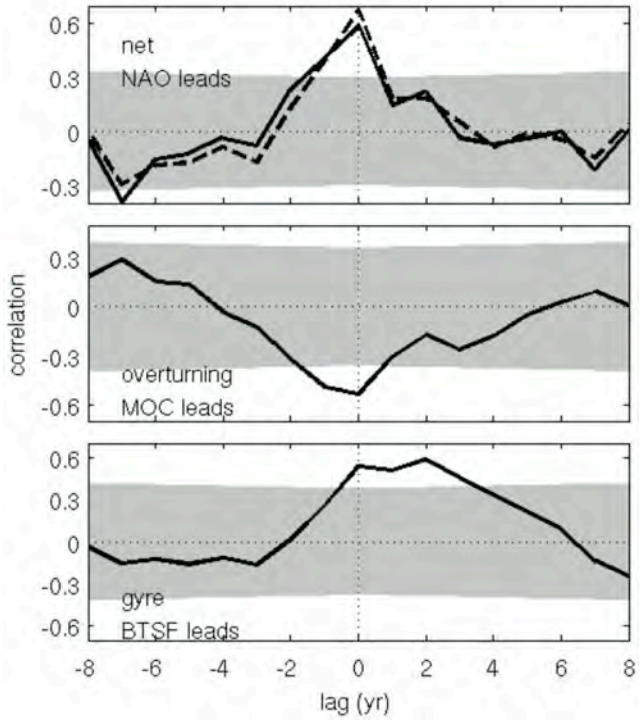

Fig. 13 Correlation between *(top)* the net freshwater transport across section A25 and the NAO, *(middle)* the overturning component of this transport and MOC PC1, and *(bottom)* the gyre component of the freshwater transport and BTSF PC1. The dashed line in the top panel indicates the cross-correlation between the freshwater transport convergence in IRM+ENA and the NAO. The shaded area indicates the 90 % confidence interval.

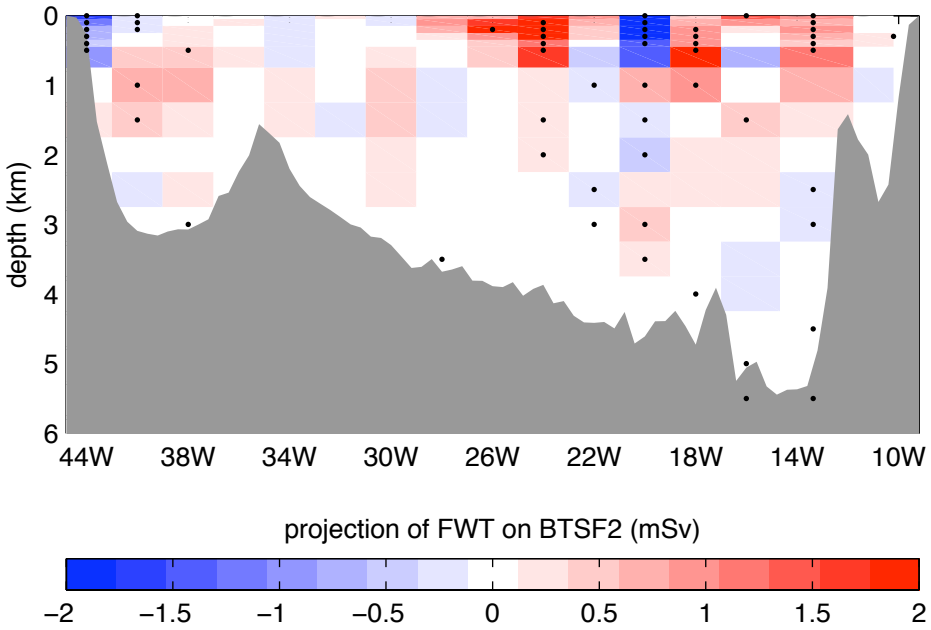

Fig. 14 Regression of the northward freshwater transport (in mSv) across A25 onto BTSF PC2, after detrending. A black dot indicates that the regression is statistically significant at the 10% level.